Supporting Online Material

Atomic structure of human adenovirus by cryoEM reveals interactions among protein networks

Hongrong Liu[1,2,3], Lei Jin[1,2], Sok Boon S. Koh[4], Ivo Atanasov[2], Stan Schein[2,5,6], Lily Wu[2,4], Z Hong Zhou[1,2,*]

[1] Department of Microbiology, Immunology and Molecular Genetics, University of California, Los Angeles (UCLA), Los Angeles, CA 90095-7364, USA

[2] California NanoSystems Institute, UCLA, Los Angeles, CA 90095-7151, USA

[3] Institute of Modern physics, Xiangtan University, Xiangtan, Hunan 411105, China

[4] Department of Molecular & Medical Pharmacology, Institute of Molecular Medicine (IMED), UCLA School of Medicine, Los Angeles, CA 90095-1735, USA

[5] Department of Psychology, UCLA, Los Angeles, CA 90095-1563, USA

[6] Brain Research Institute, UCLA, Los Angeles, CA 90095-1761, USA

[*] **Correspondence to** Hong.Zhou@ucla.edu. Phone 310.983.1033

Supporting Online Material includes:

Materials and Methods

Adenovirus preparation

The Ad-ΔE1B19/55 is an E1B gene-attenuated oncolytic adenovirus that contains wild-type Ad5 capsid, and it is constructed as previously described (*S1*). For this study, we exploited its ability to propagate to high titer in HEK 293 cells. We harvested the infected HEK 293 cells and liberated viruses by 3 cycles of freezing/thawing. Viruses were purified by CsCl step gradient ultra-centrifugation, dialyzed and resuspended in 10 mM Tris (pH 7.5), 1 mM $MgCl_2$ and 10% glycerol, and stored at -80°C prior to cryoEM imaging. The virus particle concentration was determined by spectrophotometry at 260 nm to be ~10^{12} particles/ml.

CryoEM imaging and 3D reconstruction

Frozen viral preparations were thawed, and glycerol was removed by pelleting and resuspending the viral particles in Tris buffer. Ad5 particles were embedded in a thin layer of vitreous ice suspended across the holes of holey carbon films by plunge freezing into liquid ethane. CryoEM images were recorded on Kodak SO163 films at a dosage ~20 electrons/$Å^2$ in an FEI Titan Krios cryo-electron microscope operated at 300kV and liquid-nitrogen temperature at ×59,000 nominal magnification with a defocus value between 1.0μm to 2.5μm. The films were digitized with a Nikon Super CoolScan 9000 ED scanner at 6.35 μm/pixel, corresponding to 1.076Å/pixel at the sample level.

We took a total of 1350 micrographs and selected 756 micrographs that clearly showed signals reaching 1/4$Å^{-1}$ in their spectra (Fig. S1A-C). Individual particle images (1024 pixel×1024 pixel) were first boxed out automatically by the *autoBox* program in the IMIRS package (*S2*), followed by manual screening with the EMAN *boxer* program (*S3*) to keep only the well-separated, contamination-free, intact 45000 particles.

The program *CTFFIND* (*S4*) was used to determine the defocus value and astigmatism parameters for each micrograph. We determined particle orientation, center parameters and subsequent 3D reconstruction with the IMIRS package (*S2*), enhanced by icosahedral

symmetry-adapted functions for 3D reconstruction (*S5*). We incorporated astigmatism in the CTF correction in both orientation/center refinement and 3D reconstruction steps. The IMIRS procedure was optimized, and the data processing was completed within two months by three personal computers, each with eight 2.33GHz CPUs and 16G memory.

We assessed the effective resolution with the 0.5 criterion of the reference-based Fourier shell correlation (FSC) coefficient [$C_{ref} = \sqrt{2FSC/(1+FSC)}$] as defined by Rosenthal and Henderson (*S6*). The map was either used directly to reveal low resolution features (Fig. S5E,F; Fig. S9 and movie 10) or deconvolved by a temperature factor of 300Å^2 (conventional definition) to enhance higher resolution features. The final reconstruction was filtered to 3.6Å resolution by low pass filtering with a cosine-shaped cutoff of 8 Fourier pixels (full-width at half max).

Atomic model building, model refinement and 3D visualization

We segmented and visualized the 3D map and displayed atomic models with Chimera (*S7*) before and after model building and refinement. We performed atomic modeling of individual proteins by the following procedure: First, we used an HMM (Hidden Markov Model)-based protein structure prediction algorithm (http://compbio.soe.ucsc.edu/SAM_T08/T08-query.html) to do sequence-based secondary-structure prediction. Second, we used the *Baton_build* utility in the crystallographic programs *O* (*S8*) and *Coot* (*S9*) to build C_α models. Amino-acid sequence registration was accomplished based solely on the clear densities of bulky side chains, which serve as 'landmarks' (table S2). Third, we built full-atom models with the help of *REMO* (*S10*). Fourth, we further improved the fit of the atomic model to the density map with iterative cycles of model rebuilding using *O/COOT* and geometry refinement using *O* until no obvious improvement could be obtained. Our final models match the cryoEM density well and have good geometry.

Supporting Text

Detailed Interactions of Minor Proteins

Interactions of protein IIIa.

The N-terminal helix-rich region (aa 7-300) of protein IIIa has four domains (Fig. 2B; density map in Fig. S3A). The GOS-glue domain (aa 7-105) comprises six helices (aa 10-17, 29-35, 43-47, 50-61, 71-83 and 91-105) and interacts with a penton-base monomer [Fig. 2A, lower right inset; contacts 1-3 by protein IIIa (red) in Fig. S10A schematic and table S3A], an adjacent protein IIIa (contact 4 in Fig. S10A and table S3A), and two peripentonal hexons (contacts 5 and 6 with one hexon, contact 7 with the other hexon in Fig. S10A and table S3A). The connecting-helix domain (aa 106-138) comprises a ~35Å-long helix (aa 108-132) and simply reaches from the GOS-glue domain to the VIII-binding domain. The VIII-binding domain (aa 139-251) comprises four helices (aa 138-149, 158-172, 201-211 and 230-243) and three small anti-parallel β strands (aa 178-182, 187-191 and 197-200; Fig. S3B) that interact with protein VIII (Fig. 2A, top right inset; contacts 8 and 9 in Fig. S10A and table S3A). The core-proximal domain (aa 252-300) comprises two helices (aa 252-281, 288-299) and may connect to the genome core (Fig. 5A, red circles).

Interactions of protein VIII

Protein VIII (Fig. 2C; density map in Fig. S4A) has three domains: head domain (aa 94-110 and 159-165) (~15Å long), neck domain (aa 80-93 and 166-180) (~45Å long) and body domain (aa 2-79 and 181-227) (~50Å long) (Fig. 2C). The small head domain comprises a two-turn helix, an isolated β strand, and two short loops. The long neck domain connecting the head and body includes two anti-parallel β strands and four loops. The large body domain comprises a long helix (aa 38-63; Fig. S4B) and a short helix (aa 186-190), three anti-parallel β strands, an isolated β strand, and some loops. The three anti-parallel β strands interact with protein IIIa [red in Fig. 2A, right upper inset; contacts 12 and 13 by (blue) VIII in Fig. S10A and table S3B [same as contacts 8 and 9 by (red) protein IIIa in Fig. S10A and table S3A]. The two isolated β strands

in the head and body domains (Fig. 2C) join the β sheets (Fig. 5A schematic, magenta portion of edges of monomers) of the VC region of two hexons via β-strand augmentation (Fig. 2A, top insets) at contacts 1 and 6 in Figure S10A and table S3B.

Interactions of protein IX

The protein IX monomer (Fig. 3B; density map in Fig. S5A,B) has an N-terminal domain (~50Å long) with a β hairpin (β1 and β2) and an isolated β strand (β3), a rope domain (~70Å long) with a 3-turn helix, and a helix-bundle domain with a long 12-turn helix (~65Å), all joined by loops. The N-terminal domain, specifically its β3 strand, interacts by β-strand augmentation (Fig. 3A, lower left inset) with β sheets of the FG2 region of the hexon (contacts numbered 1 in Fig. S10B schematic and in table S3C), whereas side-chain interactions are responsible for contacts numbered 2 and 3. In addition, individual rope domains (blue, yellow, green and red) make different combinations of contacts 4 and 5 with neighboring hexons (Fig. S10B and table S3C). Finally, the green helix-bundle domain crosses over the other three and interacts with a hexon (H4) (blue arrow in Fig. S5E, contact 6 onto H4 in Fig. S10B).

Supporting Online Figures

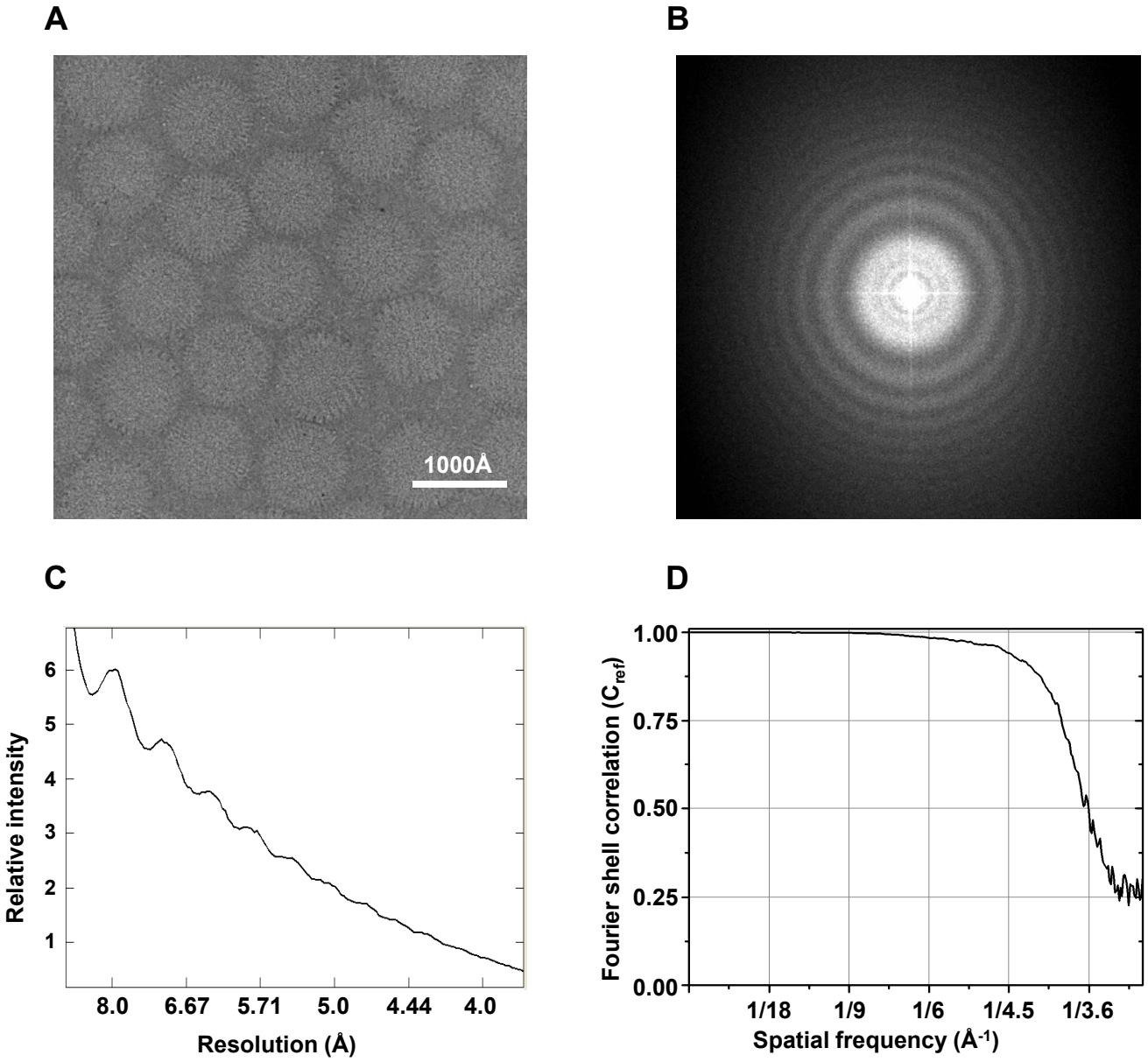

Figure S1. CryoEM image of Ad5 and resolution assessment. **(A)** Representative area of image recorded on Kodak SO163 film in an FEI Titan Krios cryo-electron microscope operated at 300kV at liquid-nitrogen temperature. **(B)** 2D power spectrum for the average of a single micrograph taken at a defocus of 1.3μm. **(C)** Rotationally averaged power spectrum for (B), showing structure-factor profile modulated by the contrast transfer function to 4Å but with a monotonic decline below that point. **(D)** Resolution assessment of the reconstruction based on the 0.5 criterion of the reference-based Fourier shell correlation coefficient [$C_{ref} = \sqrt{2FSC/(1+FSC)}$] (*S6*), showing that the effective resolution of the 3D reconstruction is 3.6Å.

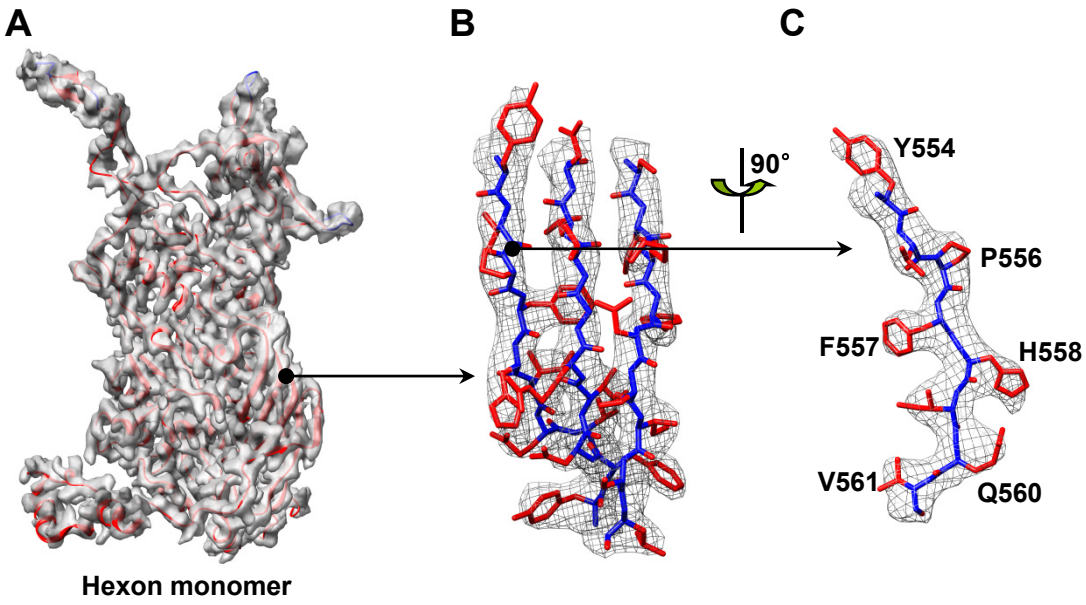

Figure S2. Hexon monomer. **(A)** Atomic model (ribbons) of a hexon monomer superimposed on its density map (semi-transparent gray).**(B)** Representative enlargements of a β sheet showing separation of strands. (**C**) One of its three strands is rotated to show side chains (labeled) that are perpendicular to the β sheet. In B and C, densities are shown as mesh, and atomic models are displayed using sticks.

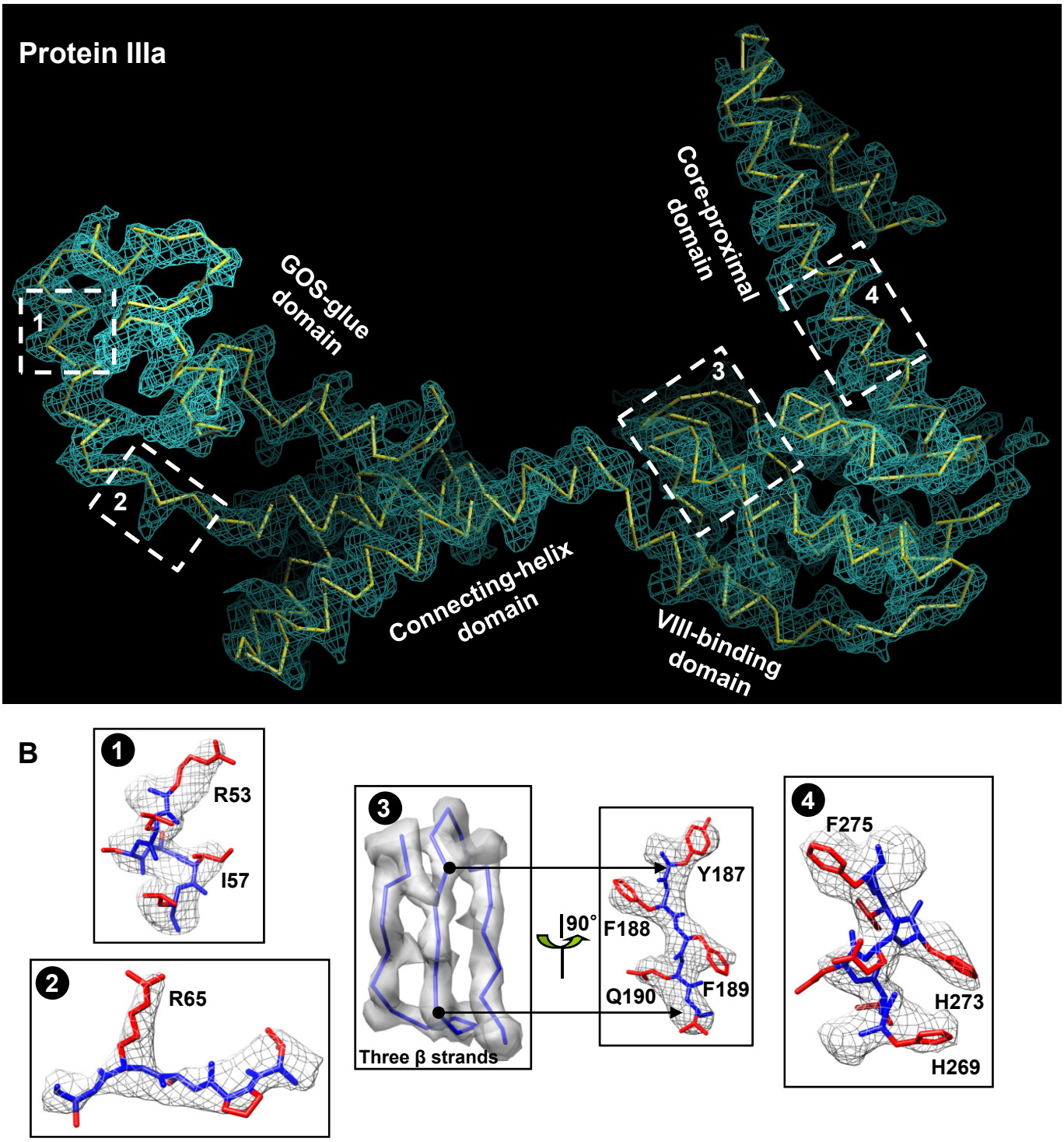

Figure S3. Protein IIIa. **(A)** Superposition of the cryoEM density map (mesh) and the backbone of the atomic model (yellow sticks). **(B)** Enlargements of boxed regions from (A), showing the density map (mesh or semitransparent gray) clothing models of amino acids. Some landmark amino acids with distinctive side chains are labeled. In (3), the density of a β sheet, shown in semitransparent gray, reveals the separation of strands. The middle strand is rotated to show side chains that are perpendicular to the plane of the β sheet. See also movie S6.

A

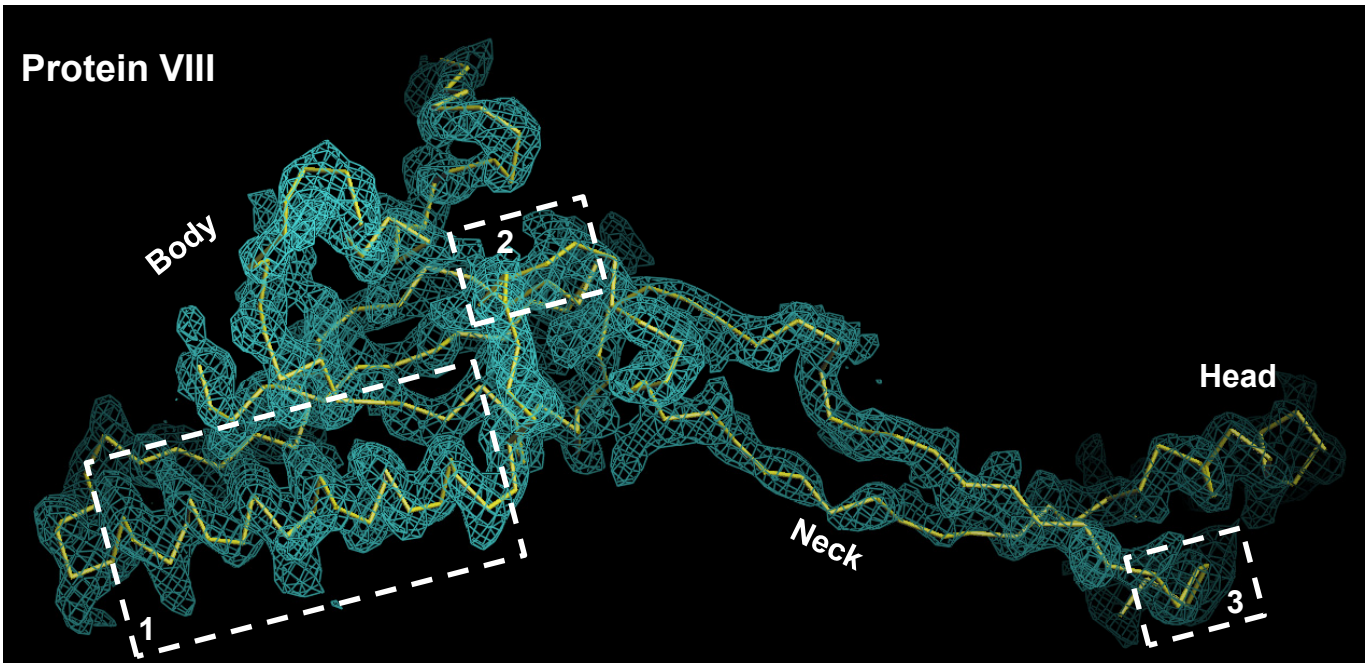

B

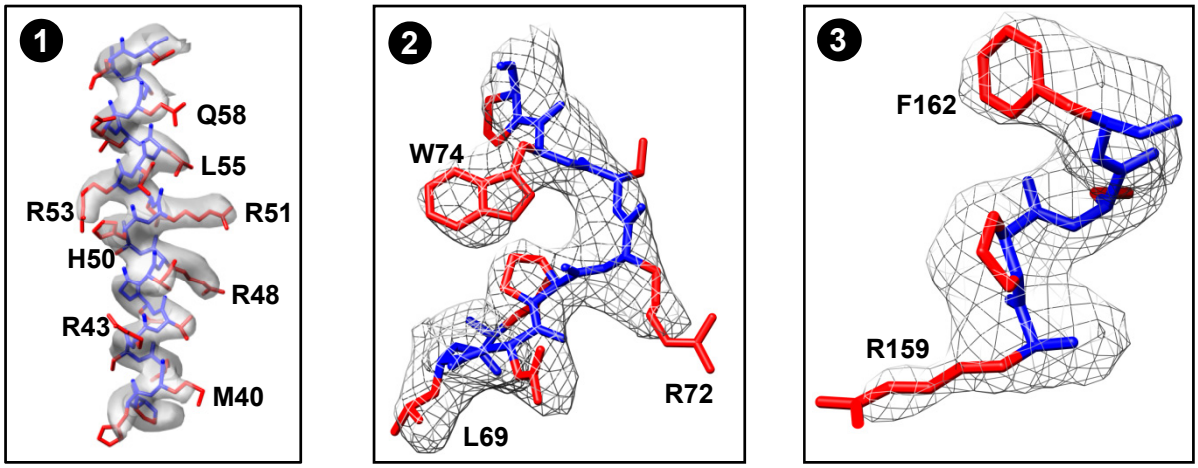

Figure S4. Protein VIII. **(A)** Superposition of the cryoEM density map (mesh) and the backbone of the atomic model (yellow sticks). **(B)** Enlargements of boxed regions from (A), showing the density map (semitransparent gray or mesh) clothing models of amino acids. Some landmark amino acids with distinctive side chains are labeled. See also movie S7.

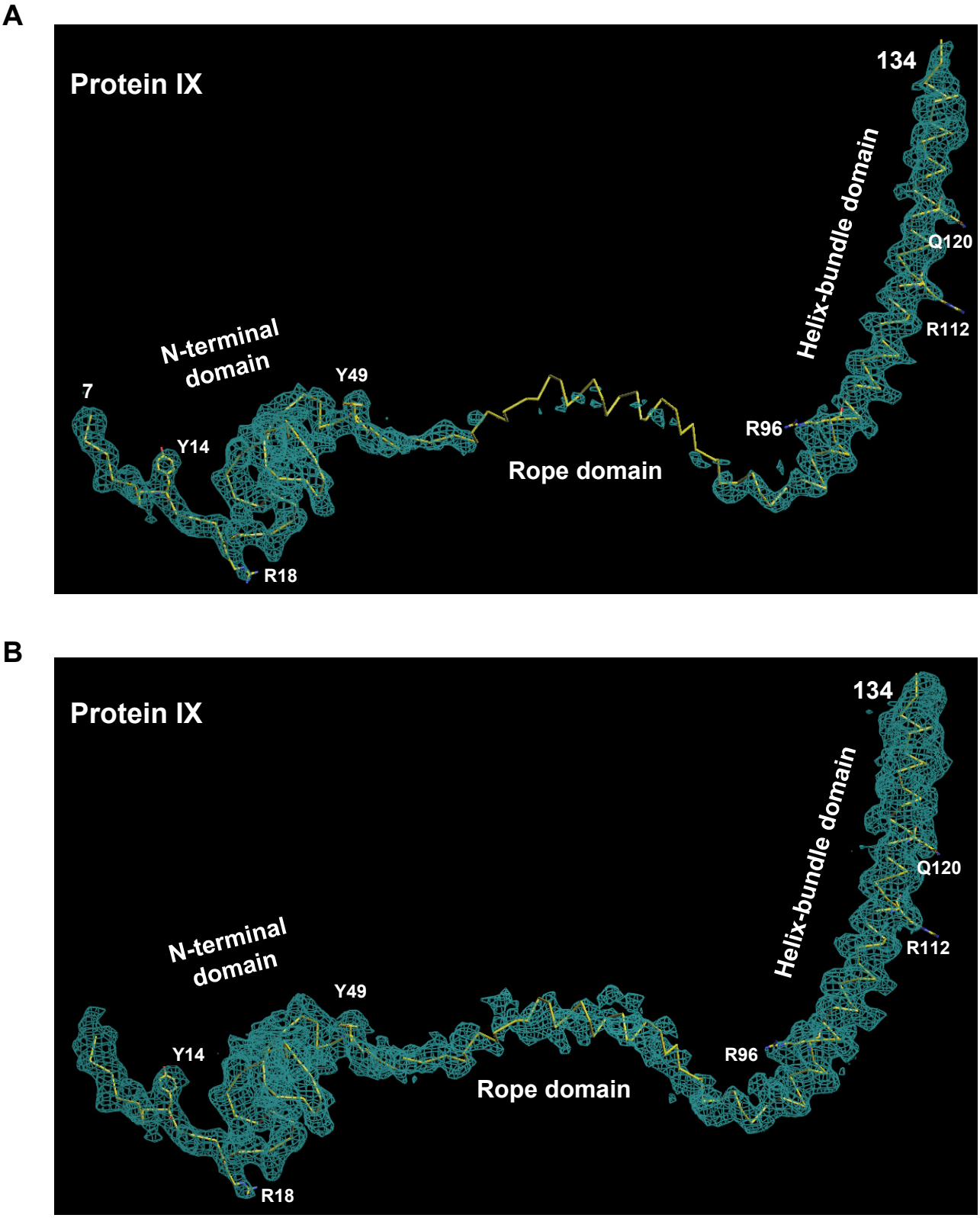

Figure S5 (A-B). Protein IX. Superposition of the cryoEM density map (mesh) displayed at relatively high threshold (**A**) and at relatively low threshold (**B**) along with the backbone of the atomic model (yellow sticks).

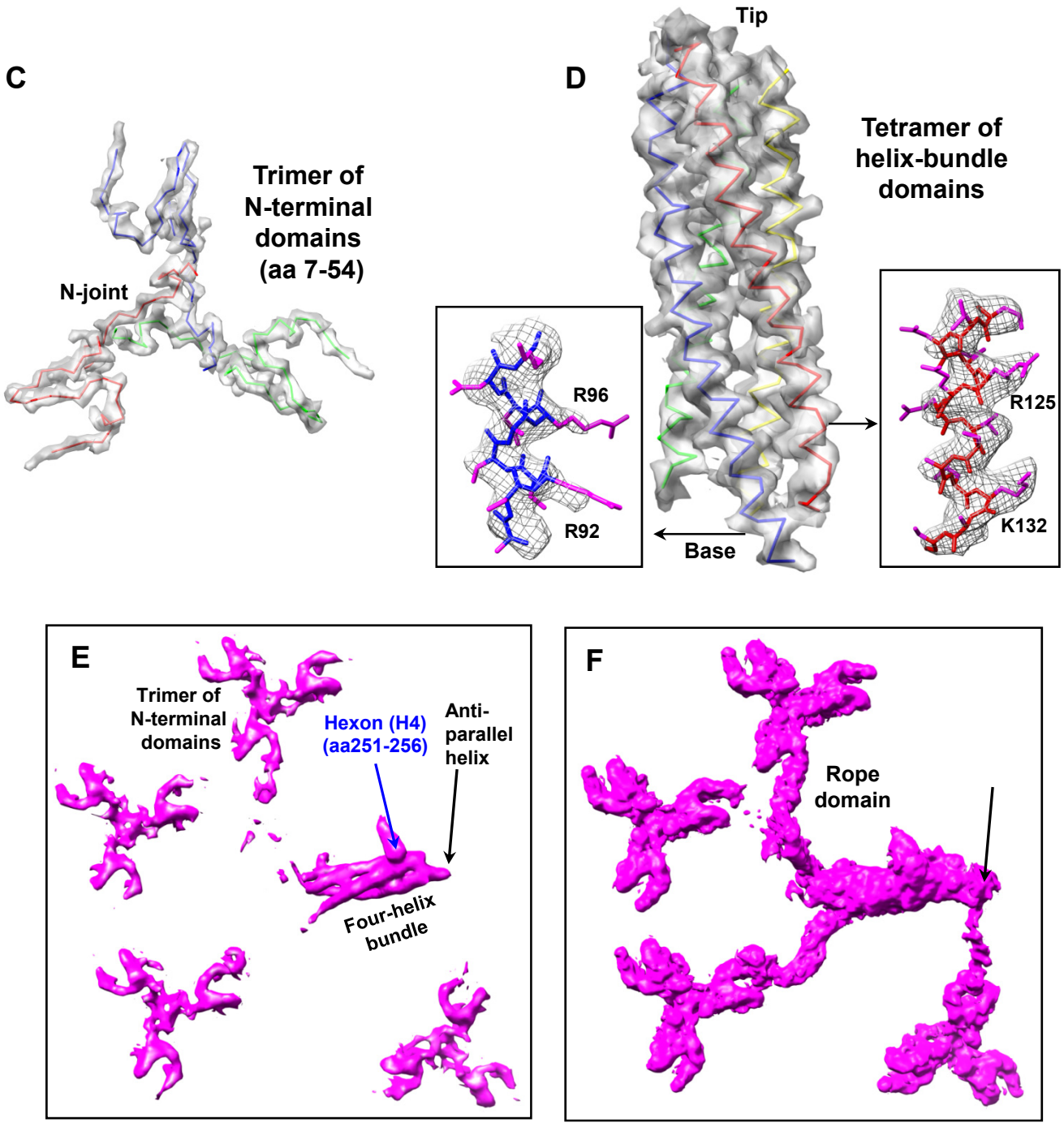

Figure S5 (C-F). Protein IX. **(C)** Density map of an N-terminus trimer (aa 7-54) See also movie S8. **(D)** Four-helix bundle, involving four C-terminus helix-bundle domains (aa 89-134 for the blue one). See also movie S9. Atomic models confirm that the red helix-bundle domain runs anti-parallel to the blue, green and yellow ones. Insets: Enlargements showing the density map (mesh) clothing models of amino acids and their side chains. **(E-F)** Densities of four trimeric N-joints and their associated four-helix bundle of protein IX displayed at relatively high (**E**) and low (**F**) density thresholds. These densities, extracted from the 3D map reconstructed using B = 0Å^2 to enhance low resolution features, show the continuity of all four rope domains (**F**). See also movie S10. The three helix-bundle domains from the left are parallel, and the one from below and to the right is anti-parallel.

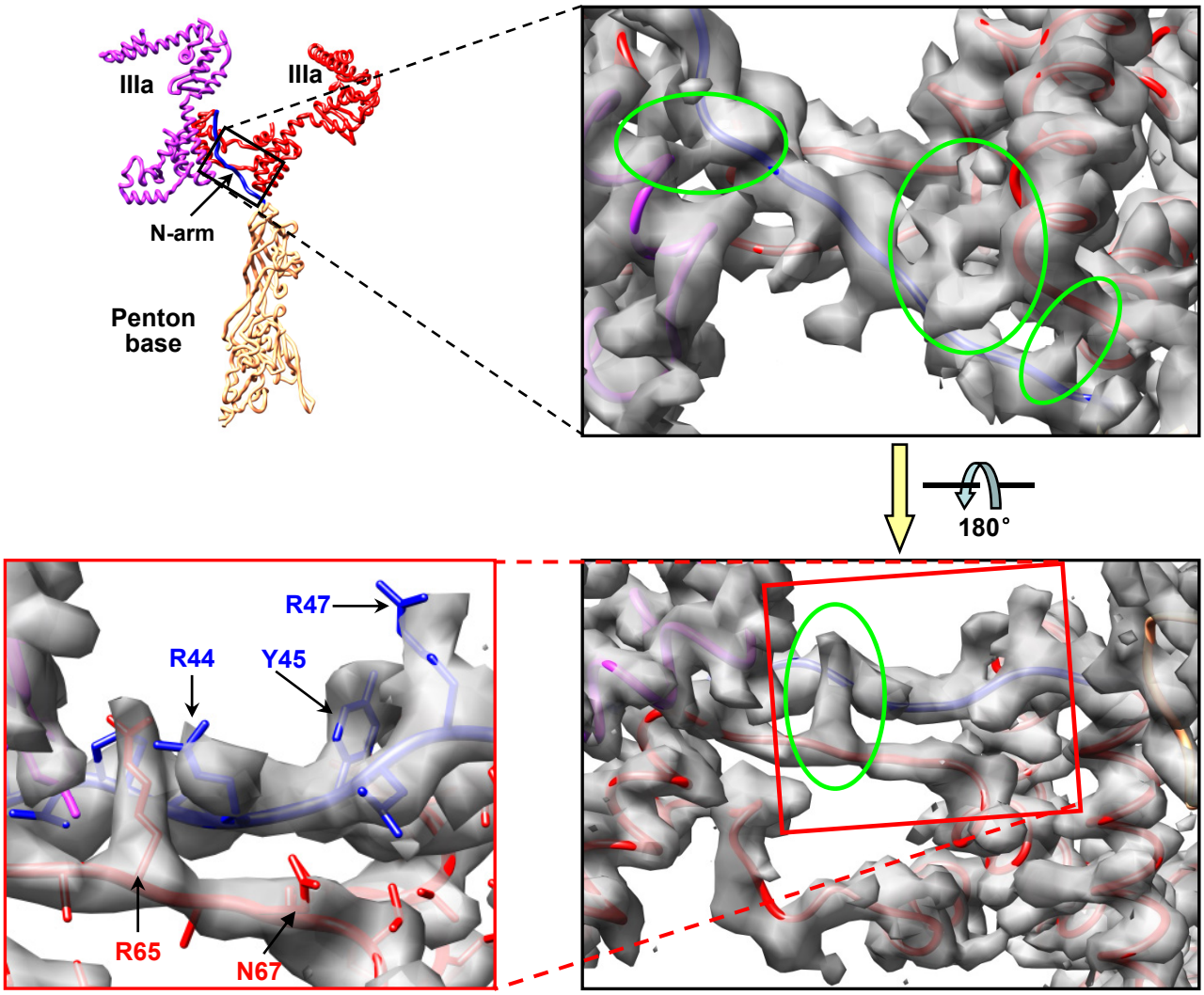

Figure S6. Interactions between the penton base and protein IIIa. The N-arm (boxed, blue loop in the ribbon model) interacts with two adjacent (magenta and red) proteins IIIa, the zones of interaction marked by green ellipses in the density map to the right, rotated below and to the right, and enlarged below and to the left.

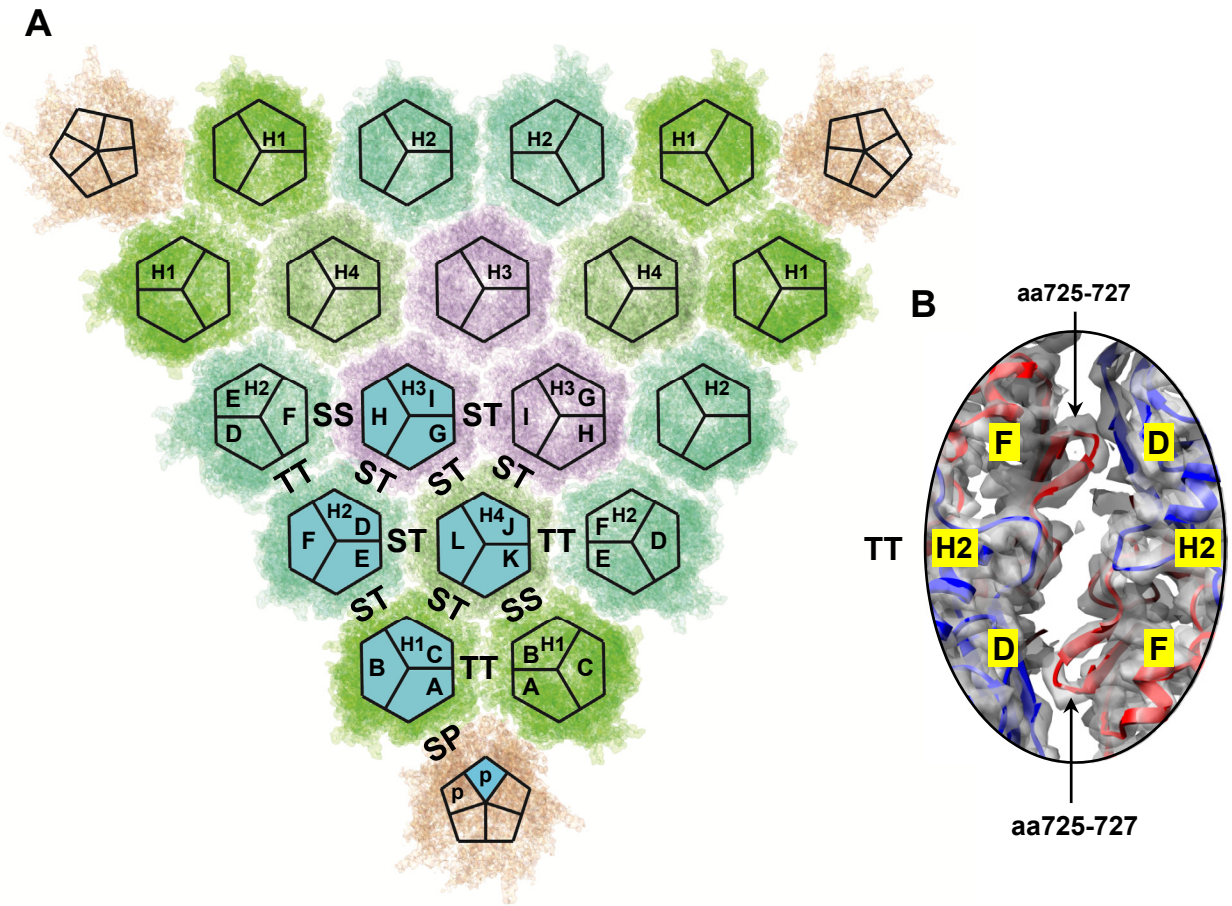

Figure S7. Interactions between major proteins. **(A)** A view of the inner surface of a facet (as in the lower panel of Fig.1B but excluding the minor proteins) shows how the sites of interaction between hexon and hexon and between hexon and penton base are coded in table S5. The 12 quasi-equivalent hexon monomers in an asymmetric unit (cyan filled) are designated A, B … J, corresponding to the main chain number in the deposited PDB model; the penton-base monomer is designated p. Hexagon sides formed by Single monomers are marked S, by Two monomers are marked T; the sides of a penton base are marked P. There are thus four kinds of interface: SS, TT, ST and SP. The body domains of protein VIII on the inner surface are located at SS interfaces (H1-H4 and H2-H3) (Fig. 5A), centered on local 2-fold axes. The four-helix bundle of protein IX occupies one of the TT interfaces (H2-H4), centered on a second kind of local 2-fold axis. **(B)** Ribbon model of two adjacent H2 monomers superimposed on their density maps (semitransparent gray), showing a weak interaction at the TT (H2-H2) interface.

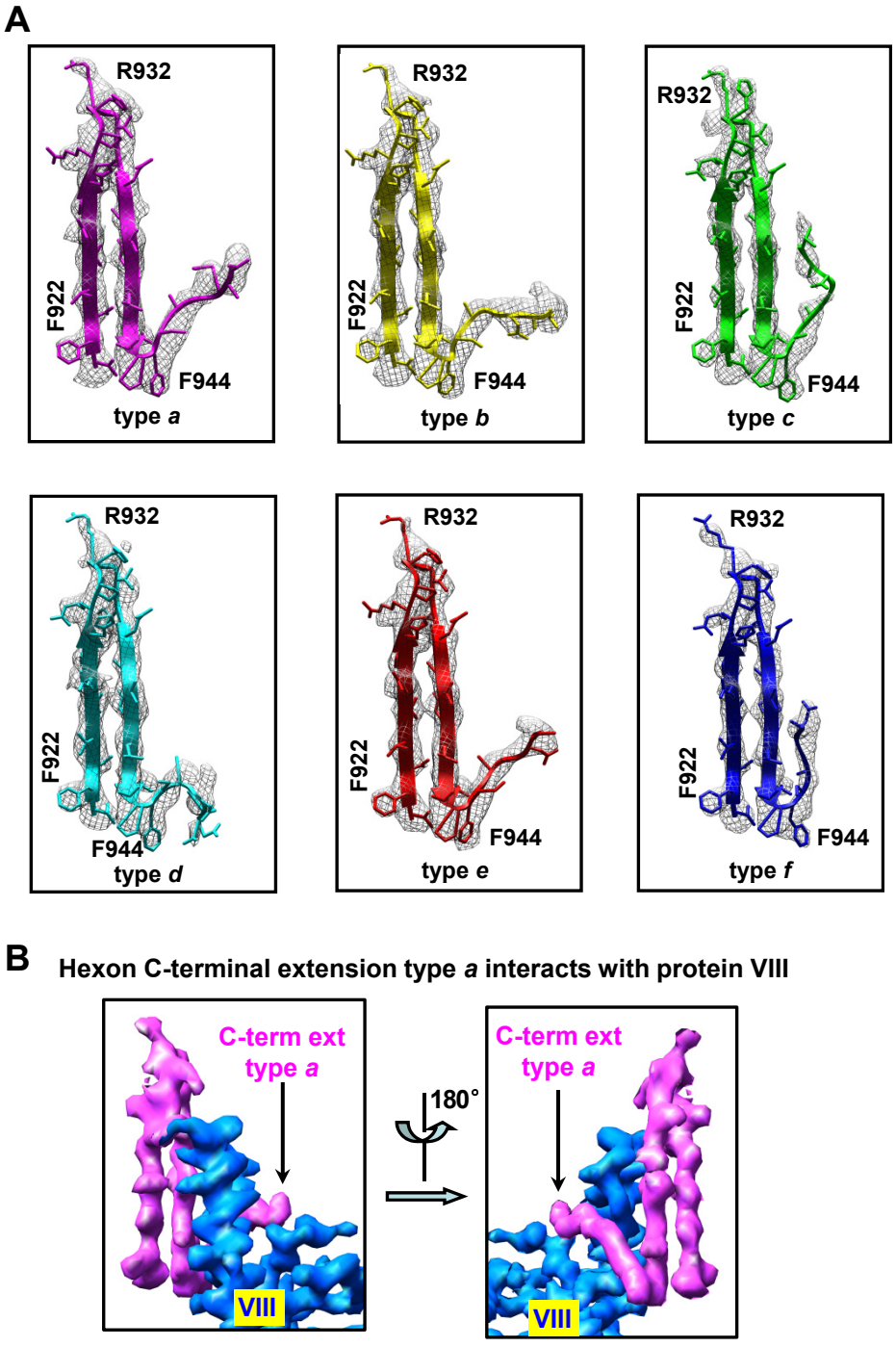

Figure S8. Conformational adaptation demonstrated by six types of hexon C-extension. **(A)** Each type of C-terminal extension, aa 944-950 of the 921-950 shown, is located on the bottom right of its hexon (Fig. 4B). **(B)** The type *a* C-extension (magenta) inserts like a hook into the body of a protein VIII (blue). By contrast, the type *b* inserts into a head, the type *c* interacts with the other side of the body, and the types *d-f* do not interact with protein VIII. The type *f* is unique in that it is adjacent to a penton monomer (Fig. 5A).

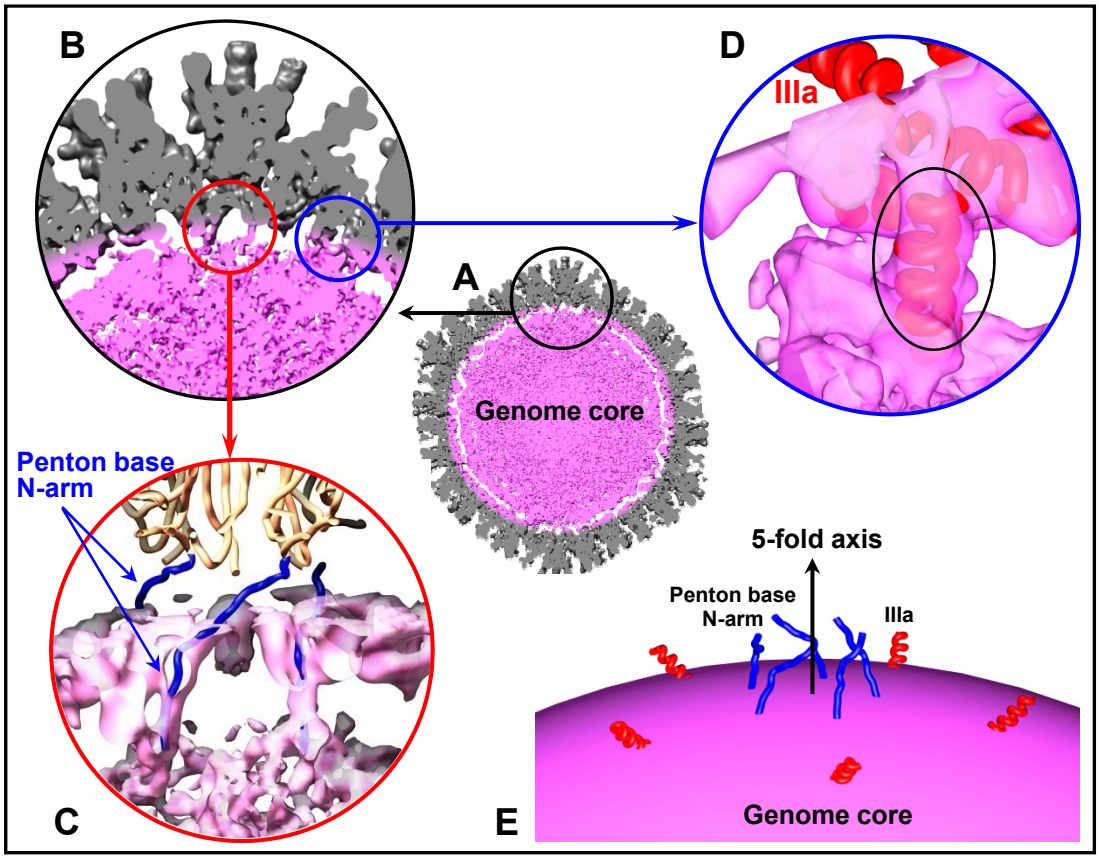

Figure S9. Connections between a GOS and the genome core. **(A)** A central slice through the two-fold axis of a virion shows that, except in the regions – one circled in black – underneath each GOS, the capsid is separated from the genome core by a gap. **(B)** Enlargement of the black-circled GOS-adjacent region from (A). **(C)** The N-arm of a penton base (blue) extends to the genome core. **(D)** A rod density – a helix of protein IIIa (black ellipse) – connects with the genome core. **(E)** The diagram shows the connections between a GOS – specifically made by protein IIIa (red) and the N-arm (blue) of the penton base – and the genome core centered on the 5-fold axis.

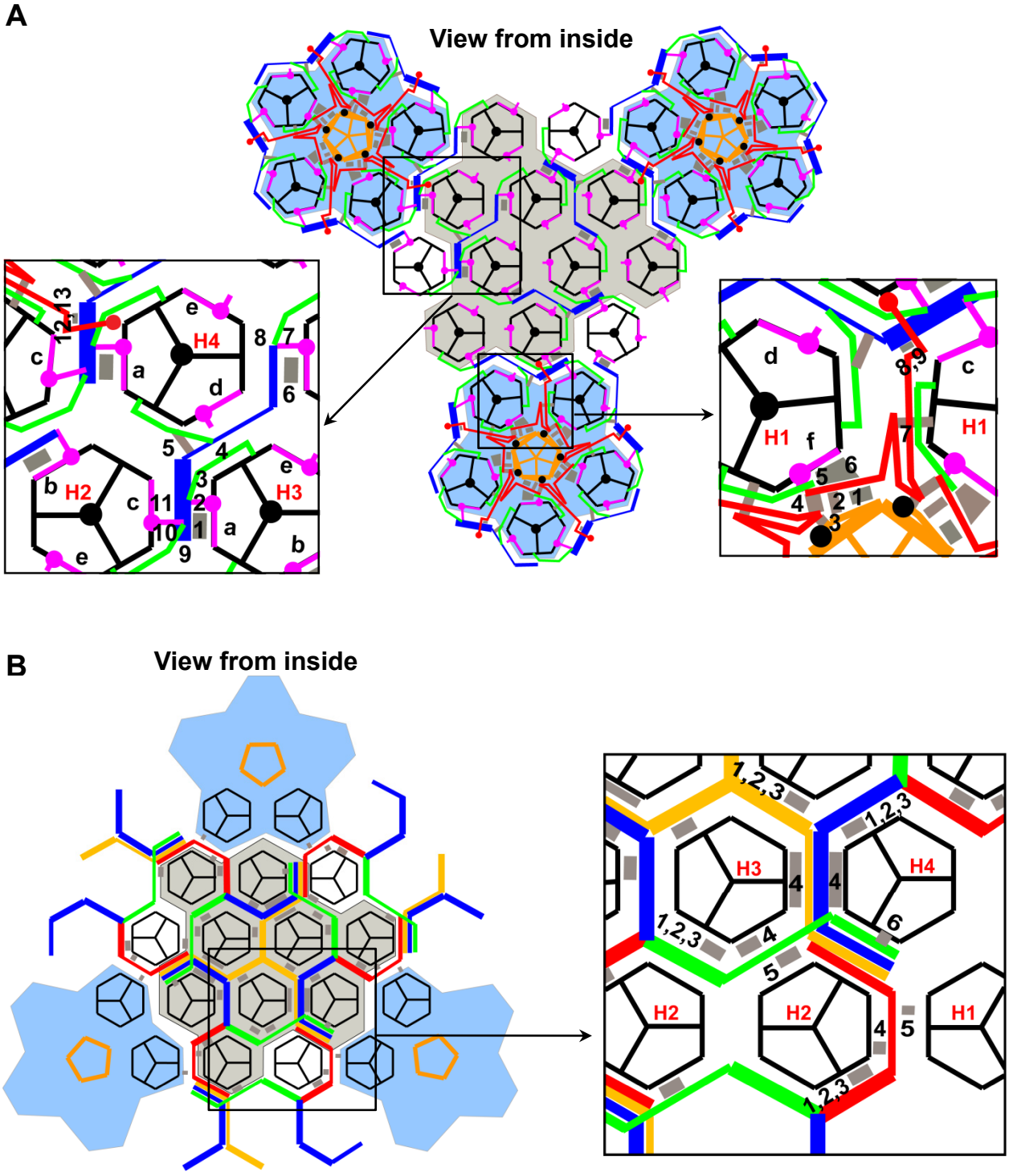

Figure S10. Numbered interaction sites on the inner surface (**A**) and on the outer surface (**B**). See Figure 5 and table S3 for additional details.

Supporting Online Tables

Table S1 Summary of capsid proteins of Ad5

	Polypeptide	Number of residues in monomer	Copy number in capsid (*S11*)	Total number of amino acids	Atomic model by X-ray crystallography	CryoEM model reported here
Major proteins	Hexon (II)	952	720	685440	yes (Ad5)	yes including extensions (aa2-7, aa251-256, aa443-444, aa944-950)
	Penton base (III)	571	60	34260	yes (Ad2)	yes including extension (aa37-51)
	Fiber (IV)	581	36	20916	yes (Ad2)	none
Minor proteins	IIIa	585	60	35100	none	yes (aa7-215, aa226-300)
	VI	250	~360	90000	none	fragmented density only
	VIII	227	120	27240	none	yes (aa3-110, aa 159-226)
	IX	140	240	33600	none	yes blue (aa7-134) red (aa7-54, aa95-137) yellow (aa7-54, aa93-130) green (aa7-54, aa98-133)

Table S2 Landmark amino acids of minor proteins IIIa, VIII and IX

Protein IIIa (Side-chain densities of 85% amino acids in our model are visible)		Trp27, Arg28, Arg33, Arg40, Phe45, Arg46, **Arg53**, **Arg65**, **His70**, Arg87, Try95, Arg101, Try105, Arg116, Arg122, Arg128, Arg130, Phe146, Tyr161, Phe164, Arg169, Try181, **Try187**, **Phe188**, **Phe189**, **Gln190**, Arg193, Phe205, Trp212, Arg233, Arg250, Try253, His256, Try261, Arg262, **His269**, **His273**, **Phe275**, Arg283
Protein VIII (Side-chains densities of 85% amino acids in our model are visible)		Lys3, Trp11, Tyr13, Tyr27, Try33, His39, **Arg43**, **Arg48**, **His50**, **Arg51**, **Arg53**, Arg66, Arg72, **Trp74**, Tyr80, Arg93, **Arg159**, **Try162**, Arg179, Phe188, Phe192, Tyr197, Phe198, Phe201, Tyr208, Phe212, Phe216
Protein IX	N-terminal domain Side-chains densities of 85% amino acids in our model are visible	**Tyr14**, **Arg18**, **Trp22**, Arg26, Tyr49
	helix-bundle domain Side-chains densities of 70% amino acids in our model are visible	**Arg92**, **Arg96**, Arg112, **Arg125**, **Lys132**
Bold: Densities of these amino acids are shown either in Figures 2-3 or SOM Figures S3-5.		

Table S3A Proposed interactions involving protein IIIa on the interior surface*

No.	IIIa			penton base			Interaction type
	Position	Secondary structure	Amino acids	Position	Secondary structure	Amino acids	
Between protein IIIa and the penton base							
1	GOS-glue domain		Gly108-Thr112	N-arm		Tyr45	
2	GOS-glue domain		Arg65	N-arm		Pro42-Pro43	
3	GOS-glue domain	helix	Pro63-Ala64 (one protein IIIa) Leu114-Val 110 (adjacent IIIa)	N-arm	loop	Pro38-Val41	mostly hydrophobic
Between proteins IIIa and adjacent IIIa							
	IIIa			adjacent IIIa			Interaction type
	Position	Secondary structure	Amino acids	Position	Secondary structure	Amino acids	
4	GOS-glue domain	helix	Ile86-Ala124	GOS-glue domain	helix and loop	Met35-Val61	mostly hydrophobic
Between protein IIIa and hexon							
	IIIa			hexon			Interaction type
	Position	Secondary structure	Amino acids	Position	Secondary structure	Amino acids	
5	GOS-glue domain	loop and helix	Pro18-Leu21	NT (H1)	helix	Met5-Pro25	mostly hydrophobic
6	GOS-glue domain	helix	Ala91-Leu99	VC (H1)	helix	Ala626-Ala 631	mostly hydrophobic
7	connecting-helix	helix	Leu93-Ala97	V2 (H1)	helix	Leu891-Ala894	mostly hydrophobic
Between proteins IIIa and VIII							
	IIIa			VIII			Interaction type
	Position	Secondary structure	Amino acids	Position	Secondary structure	Amino acids	
8	VIII-binding domain	strand	Leu196-Asn200	belly domain	strand	Ser195-Phe 198	β-strand integration
9	VIII-binding domain	loop and strand	Glu179-Tyr181, Gln190-Thr198	belly domain	loop	Ser202-Pro209	

* All these sites have at least one visible density contact between amino-acid side chains, see one example in Fig. S6.

Table S3B Proposed interactions involving protein VIII on the interior surface*

No.	VIII				Hexon			Interaction type
	Position	Secondary structure	Amino acids		Position	Secondary structure	Amino acids	
Between protein VIII and hexons inside a GON								
1	belly domain	strand	Arg30-Asn32		VC (H3)	β strand	Val938-Thr942	β-strand integration
2	belly domain	loop,helix	Arg30-Ala49		C-term extension (H3)	loop	Phe944 -Thr950	
3	belly domain	helix	Arg43-His50		N terminal (H3)	helix	Met6-Met12	mostly hydrophobic
4	neck domain	loop	Pro178-Leu183		N terminal (H4)	helix	Met5-Gln17	mostly hydrophobic
5	neck domain	loop	Ser174-Glu177		N terminal (H4)	helix	Glu21-Pro25	
6	head domain	strand	Gly105-Ala109		VC (other H3)	strand	Val938-Thr942	β-strand integration
7	head domain	helix	Thr102-Gly105		C-term extension (H3)	loop	Phe944-Thr950	
8	head domain	helix	Ser161-Phe162, Ala104-		N terminal (H3)	helix	Met5-Tyr11	mostly hydrophobic
Between protein VIII and hexons outside the GON								
9	belly domain	loop	Pro200-Pro205		N terminal (H2)	helix	Pro25-Val28	
10	belly domain	loop, helix	Met34-Ile41		N terminal (H2)	helix	Met5-Pro7	mostly hydrophobic
11	belly domain		Ile31-Ser35		VC (H2)		Gly947-Thr950	
Between proteins VIII (around the 5-fold axis) and IIIa								
	VIII				IIIa			Interaction type
	Position	Secondary structure	Amino acids		Position	Secondary structure	Amino acids	
12	belly domain	strand	Ser195-Phe198		VIII-binding	strand	Leu196-Asn200	β-strand integration
13	belly domain	loop	Ser202-Pro209		VIII-binding	loop and strand	Glu179-Tyr181, Gln190-Thr198	

* All these sites have at least one visible density contact between amino-acid side chains, see one example in Fig. S6.

Table S3C Proposed interactions involving protein IX on the exterior surface*

Between protein IX and hexons									
Four-copies protein IX	No.	IX				Hexon			
		Position	Secondary structure	Amino acids		Position	Secondary structure	Amino acids	Interaction type
Blue	1	N-termineal damain	β sheet	Tyr49-Ser53		FG2 (H4)	β sheet	Ile858-Lys862	β-strand integration
	2	N-termineal damain		Tyr 49		FG2 (H4)		Thr859-Lys861	
	3	N-termineal damain		Leu47-Glu50		FG2 (H4)		Ile744-Arg746	
	4	rope domain	loop and helix	Thr55-Arg73		One H4 monomer: Along regions V2, FG1 to V1	helices, strands & loops		mostly hydrophobic
Yellow	1	N-termineal damain	β sheet	Tyr49-Ser53		FG2 (H3a)	β sheet	Ile858-Lys862	β-strand integration
	2	N-termineal damain		Tyr 49		FG2 (H3a)		Thr859-Lys861	
	3	N-termineal damain		Leu47-Glu50		FG2 (H3a)		Ile744-Arg746	
	4	rope domain	loop and helix	Thr55-Arg73		H3b monomer (along V1) to H3c monomer (V2)	helices, β strands & loops		mostly hydrophobic
Green	1	N-termineal damain	strand	Tyr49-Ser53		FG2 (H3)	strand	Ile 858-Lys 862	β-strand integration
	2	N-termineal damain		Tyr49		FG2 (H3)		Thr859-Lys861	
	3	N-termineal damain		Leu47-Glu50		FG2 (H3)		Ile744-Arg746	
	4	rope	loop			V1 (H3)	β sheet		mostly hydrophobic
	5	rope domain	loop and helix			V1 (H2)	β sheet		mostly hydrophobic
	6	helix-bundle domain	helix	Gln126-Ala133		DE1 (protrusion, H4)	loop	Gln252-Lys256	

Table S3C (Continued)

Red	1	N-termineal damain	β3 strand	Tyr49-Ser53		FG2 (H2)	strand	Ile 858-Lys 862	β-strand integration
	2	N-termineal damain		Tyr49		FG2 (H2)		Thr859-Lys861	
	3	N-termineal damain		Leu47-Glu50		FG2 (H2)		Ile744-Arg746	
	4	rope	loop			V1 (H2)			mostly hydrophobic
	5	rope	loop			FG1 (H1)			

Among the four copies of protein IX						
	No.	Position	Secondary structure		Amino acids	Interaction type
N-knot	1	three-fold axis (three yellow copies)	loop		Tyr14, Leu15	hydrophobic
	2	pseudo-three-fold axes (three copies, blue, green and red)	loop		Tyr14, Leu15	hydrophobic
Four-helix bundle	3	channel between H4 and H2	coiled-coil (four-helix bundle)		Leu100, Lue103, Leu107, Leu114, Val117, Leu121, Leu124, Val128, Leu131	hydrophobic, see Table S4

* All these sites have at least one visible density contact between amino-acid side chains, see one example in Fig. S6.

Table S4 Ladders of amino acids underying hydrophobic interactions between pairs of helix-bundle domains (blue and red, red and yellow, yellow and green, and green and blue) of protein IX.

Blue	Red	Yellow	Green	Blue
Leu100	Leu131	Leu100	Leu100	Leu100
Leu103	V128	Leu103	Leu103	Leu103
Leu107	Leu124	Leu107	Leu107	Leu107
Leu110	Leu121	Leu110	Leu110	Leu110
Leu114	Val117	Leq114	Leu114	Leu114
Val117	Leu114	Val117	Val117	Val117
Leu121	Leu110	Leu121	Leu121	Leu121
Leu124	Leu107	Leu124	Leu124	Leu124
Val128	Leu103	Val128	Val128	Val128
			Leu131	Leu131

Table S5 Proposed interactions between hexon and hexon and between hexon and penton base*

ST												
H2		H1		H1		H4		H4		H2		
E	Thr341-Asn343	B	Leu737-Asn740	C	Thr341-Asn343	K	Asp749-Gly750	L	Thr341-Asn343	D	Leu737-Asn740	
	Ile666-Arg669		Pro667-Ser668 Asp725-Ser726 His898-Ala899		Pro667-Asn670		Pro663-Ser665		Ile666-Arg669		Pro667-Ser668 Asp725-Ser726 His898-Ala899	
	Val70-Glu73	C	Ile68-Val70		Gln350-Leu354	L	Leu65-Ile68		Val70-Glu73	E	Ile68-Val70	
	Ala351-Leu354		Gly88-Asp89						Gln350-Leu354		Gly88-Asp89	

ST												
H2		H3		H3		H4		H4		H3		
D	Thr341-Asn343	G	Leu737-Asn740	G	Thr341-Gly342	L	Thr738-Asn740	J	Gly342-Asn343	H	Asp749-Gly750	
	Ile666-Arg669		Pro667-Ser668 Asp725-Ser726 His898-Ala899		Pro667-Arg669		Pro667-Ser668 His898-Ala899		Pro667-Asn670		Pro663-Ser665	
	Val70-Glu73	H	Ile68-Glu71		Val70-Arg73	J	Ile68-Val70		Ala351-Leu354	I	Leu65-Phr67	
	Ala351-Leu354		Gly88-Asp89		Ala351-Leu354		Gly88-Asp89					

ST			
H3		H3	
I	Thr341-Gly342	I	Leu737-Asn740
	Ile666-Arg669		Pro667-Ser668 Asp725-Ser726 His898-Ala899
	Val70-Glu73	G	Ile68-Val70
	Gln350-Leu354		Gly88-Asp89

Table S5 (Continued)

TT												
local 2-fold axis				local 2-fold axis				2-fold			
H1		H1		H2		H4		H2		H2	
A	Leu65-Val70	A	Asp725-Ser728	E	Gly732-Asp734	J	Gly732-Asp734	D	Leu65-Phe68	F	Asp725-Ser727
	Thr84-Asp89		Leu891-Ala899		Asp725-Val728	K	Leu65-Ile68	F	Asp725-Ser727	D	Leu65-Phe68
	Pro575-Ser577		Asn895-His898		Leu892-Ala897		Gly88-Asp89 Gly576-Ser577		Thr738-Asn740	F	Thr738-Asn740
	Arg932-Gly933		Asn895-Ser896	F	Arg59-Gln61 Ala86-Gly88	J	Asp725-Asp734				
	Asp58-Arg61	B	Asp58-Ser60		Asp58-Gln61	K	Asp58-Gln61				
C	Gly732-Asn740	A	Gly732-Asp734								
	Gly732-Asp734	B	Arg59-Ser60								

SS								SP			
local 2-fold axis				local 2-fold axis				H1		P	
H1		H4		H2		H3		A	Gln350-Gln353	p	Glu59-Ala61
B	Ser340-Met344	K	Ser692-Pro696	F	Thr341-Met344	H	Ser692-Pro696		Leu360-Asp362	p	Ser107-Thr108
	Ala351-Leu354		Ser665-Pro667		Gln350-Ala351		Ser665-Pro667		Ser689-Asp695		Ser81-Gln85
	Val358-Leu360		Thr341-Asn342		Val358-Leu360		Thr341-Gly342				
	Pro667-Asn670		Val70-Asp71 Gln350-Gln353		Ile666-Asn670		Val70-Asp71 Gln350-Gln353				
	Gly691-Ser692		Ala76-Tyr77		Ala894-Ala897		Gln350-Gln353				
	Asn895-Ala897		Gln350-Gln353								
	His931-Gly933		Pro667-Ser668								

Following Figure S7: ST, TT, SS and BP mark the four kinds of interface between hexon and hexon and between hexon and penton base. The letters A, B, ..., J mark the 12 hexon monomers in an asymmetric unit. The letter p indicates a penton-base monomer.

* Interacting amino acid residues are defined as those that are within a distance of 7Å from each other. Among all of these interacting amino acids, the only visible, direct side-chain contacts are the three that are colored blue.

Supporting Online Movies

Movie S1 Radially colored surface view of the Ad5 reconstruction.

Movie S2 A triangular facet of the reconstructed density map of the icosahedral Ad5 capsid, starting with the outer surface – showing four types of hexon in different colors, protein IX (magenta), penton base (straw) and penton fiber (gray) – and rotating around to the inner surface – showing proteins IIIa (red), VI (yellow) and VIII (blue).

Movie S3 Example of an α helix from a hexon. The atomic model (stick) is superimposed on its cryoEM density map (mesh), starting in the same orientation as in Figure 1C. Note that all of the side chains are resolved.

Movie S4 Example of β strands from a hexon. The atomic model (stick) is superimposed on its cryoEM density map (mesh), starting in the same orientation as in Figure S2B. Note that the β strands are separated from one another and that the side chains are perpendicular to the plane of the β sheet.

Movie S5 Superposition of the atomic model (ribbon) of a hexon monomer on its semi-transparent, gray, cryoEM density map, starting in the same orientation as in Figure S2A.

Movie S6 Protein IIIa. The backbone of its atomic model is superimposed on its semi-transparent, gray, cryoEM density map, starting in the same orientation as in Figure 2B.

Movie S7 Protein VIII. The backbone of its atomic model is superimposed on its semi-transparent, gray, cryoEM density map, starting in the same orientation as in Figure 2C.

Movie S8 The N-terminal trimer of protein IX, showing the N-joint. The backbones of the atomic models of the three contributing monomers (blue, red, and green sticks) are superimposed on their semi-transparent, gray, cryoEM density maps, starting in the same orientation as in Figure S5C.

Movie S9 The C-terminal four-helix bundle of protein IX. The backbone of the atomic models of the four contributing monomers (yellow, blue, and green sticks in one direction; red stick in the anti-parallel direction) are superimposed on their semi-transparent, gray, cryoEM density maps,

starting in the same orientation as in Figure S5D.

Movie S10 Visualization of the rope domains of all four proteins IX by decreasing the density threshold of surface rendering. This density map was reconstructed with a B = 0Å^2 to emphasize low-resolution features such as those (like the protein IX rope domain) with resolution degraded by modest flexibility, starting in the same orientation as in Figure S5E,F.

References

S1. J. Kim, J. Y. Cho, J.-H. Kim, K. C. Jung, C.-O. Yun, Evaluation of E1B gene-attenuated replicating adenoviruses for cancer gene therapy. *Cancer Gene Ther.* **9**, 725 (2002).

S2. Y. Liang, E. Y. Ke, Z. H. Zhou, IMIRS: a high-resolution 3D reconstruction package integrated with a relational image database. *J. Struct. Biol.* **137**, 292 (2002).

S3. S. J. Ludtke, P. R. Baldwin, W. Chiu, EMAN: Semiautomated software for high-resolution single-particle reconstructions. *J. Struct. Biol.* **128**, 82 (1999).

S4. J. A. Mindell, N. Grigorieff, Accurate determination of local defocus and specimen tilt in electron microscopy. *J. Struct. Biol.* **142**, 334 (2003).

S5. H. Liu *et al.*, Symmetry-adapted spherical harmonics method for high-resolution 3D single-particle reconstructions. *J. Struct. Biol.* **161**, 64 (2008).

S6. P. B. Rosenthal, R. Henderson, Optimal determination of particle orientation, absolute hand, and contrast loss in single-particle electron cryomicroscopy. *J. Mol. Biol.* **333**, 721 (2003).

S7. E. F. Pettersen *et al.*, UCSF Chimera--a visualization system for exploratory research and analysis. *J. Comput. Chem.* **25**, 1605 (2004).

S8. T. A. Jones, J. -Y. Zou, S. W. Cowan, M. Kjeldgaard, Improved methods for building protein models in electron density maps and the location of errors in these models. *Acta Cryst.* **A47**, 110 (1991).

S9. P. Emsley, K. Cowtan, Coot: model-building tools for molecular graphics. *Acta Cryst.* **D60**, 2126 (2004).

S10. Y. Li, Y. Zhang, REMO: A new protocol to refine full atomic protein models from C-alpha traces by optimizing hydrogen-bonding networks. *Proteins* **76**, 665 (2009).

S11. P. L. Stewart, S. D. Fuller, R. M. Burnett, Difference imaging of adenovirus: bridging the resolution gap between x-ray crystallography and electron microscopy. *EMBO J.* **12**, 2589 (1993).